Comput Mech (2009) 43:687–700
DOI 10.1007/s00466-008-0338-3

ORIGINAL PAPER

A computationally efficient method for the buckling analysis of shells with stochastic imperfections

Vissarion Papadopoulos · Dimos C. Charmpis · Manolis Papadrakakis

Received: 11 January 2008 / Accepted: 6 September 2008 / Published online: 2 October 2008

Abstract A computationally efficient method is presented for the buckling analysis of shells with random imperfections, based on a linearized buckling approximation of the limit load of the shell. A Stochastic Finite Element Method approach is used for the analysis of the "imperfect" shell structure involving random geometric deviations from its perfect geometry, as well as spatial variability of the modulus of elasticity and thickness of the shell, modeled as random fields. A corresponding eigenproblem for the prediction of the buckling load is solved at each MCS using a Rayleigh quotient-based formulation of the Preconditioned Conjugate Gradient method. It is shown that the use of the proposed method reduces drastically the computational effort involved in each MCS, making the implementation of such stochastic analyses in real-world structures affordable.

Keywords Buckling analysis of shells · Random imperfections · Stochastic finite element · Random eigenvalues · Preconditioned Conjugate Gradient method

V. Papadopoulos (✉) · M. Papadrakakis
Institute of Structural Analysis and Seismic Research, National Technical University, 15780 Athens, Greece
e-mail: vpapado@central.ntua.gr

M. Papadrakakis
e-mail: mpapadra@central.ntua.gr

D. C. Charmpis
Department of Civil and Environmental Engineering, University of Cyprus, 75 Kallipoleos Str., P.O. Box 20537, 1678 Nicosia, Cyprus
e-mail: charmpis@ucy.ac.cy

1 Introduction

Buckling behaviour of shells is generally dominated by their initial geometric imperfections, which are usually produced during the manufacturing procedure. Early studies on the subject were mainly focused on the treatment of geometric imperfections with the Donnell-type theory together with Galerkin approximations of the solution which provided asymptotically accurate estimations at the bifurcation points [1–9]. In addition to initial geometric imperfections, other sources of imperfections such as material and thickness variability, imperfect boundary conditions, loading misalignment, etc. are proved to be of great importance as well [2–4,6–12]. In an effort to obtain reasonable predictions of the scatter of the buckling loads with respect to corresponding experimental measurements, recent studies implemented the Finite Element method in conjunction with a stochastic description of the uncertainties involved (SFEM) in all kinds of previously mentioned imperfections [13–18].

The main difficulty of the aforementioned type of SFEM approaches has always been that they can provide reasonable estimates of the scatter of the buckling loads only if the full probabilistic characteristics (marginal pdfs and correlation structures) of the involved stochastic fields are derived on the basis of corresponding experimental surveys. In the majority of engineering problems, however, there is a lack of experimental measurements for a reliable description of the statistical properties of the involved stochastic fields used for modeling the uncertain parameters [19]. In order to handle such problems, a computationally expensive sensitivity analysis is usually required with respect to the assumed parameters used for the description of the stochastic fields. Such sensitivity analysis is the only reliable way to perform the design of structures in the presence of uncertainties or to assess the structural integrity of existing structures: by

performing parametric investigations leading to the identification of "worst case" scenarios with respect to selected response quantities. On these lines, a methodology for the achievement of an optimum design has been recently proposed in [20], where results of such sensitivity analysis were used in a reliability-based sizing-shape optimization of shell-type structures with random initial geometric material and thickness imperfections, along with a technique for modeling the geometric boundary imperfections when experimental measurements are unavailable [16]. The main disadvantage of both aforementioned approaches is the enormous computational time involved in the repeated MCS required for performing parametric investigations.

In the present study a computationally efficient method is presented for the buckling analysis of shells with random imperfections. The proposed methodology is based on a linearized buckling approximation of the limit load of the shell, which is formulated in the framework of a Monte Carlo Simulation procedure. A SFEM approach is used for the analysis of the "imperfect" shell structure involving random geometric deviations from its perfect geometry, as well as spatial variability of the modulus of elasticity and thickness of the shell. The involved uncertain parameters are modeled as stochastic fields. A corresponding eigenproblem is solved at each MCS using a Rayleigh quotient-based formulation of the Preconditioned Conjugate Gradient (PCG) method. The proposed methodology is particularly suitable in cases where a computationally expensive sensitivity analysis is required with respect to assumed parameters used for the description of the stochastic fields. It is shown that the use of the proposed method reduces drastically the computational effort involved in each MCS, making the implementation of this type of stochastic analyses in real-world structures affordable. Furthermore, it is shown that the proposed approach provides close estimates of the buckling loads with respect to the "exact" ones obtained via a more accurate incremental-iterative nonlinear analysis.

In order to numerically demonstrate the validity of the proposed methodology, two types of shell structures are selected based on their buckling behaviour up to their limit point. The first shell is a shallow hinged isotropic cylindrical panel with a point load at the apex. This shell exhibits a limit point buckling with relatively large pre-buckling deformations. The second shell is a thin-walled isotropic axially compressed cylinder, which exhibits a bifurcation buckling mode under small deformation. This type of shell is selected as an example of an imperfection-sensitive structure in the sense that small deviations from its perfect geometry may result in a dramatic reduction of its buckling strength, while the first type of shell was selected as representative of a less sensitive to initial imperfections type of shells. It is shown that in both cases the proposed approach achieves close estimates of the first and second order moments of the buckling loads, as well as of the shape of their distribution, with respect to the corresponding "exact" results obtained via an incremental-iterative nonlinear analysis.

2 Random geometric imperfections

Two different approaches are used for modeling the random initial imperfect geometries of the two selected types of shell structures. The reason for this distinction is that in the case of the cylindrical panel (Fig. 1), no experimental data is available for a statistical quantification of random initial geometric imperfections, while in the case of the axially compressed cylinder (Fig. 8), the imperfect geometry is derived based on available experimental measurements.

2.1 Imperfect geometry of the cylindrical panel

The imperfect geometry of the cylindrical panel of Fig. 1 is modeled as a two-dimensional univariate (2D-1V) homogeneous Gaussian stochastic field. The assumption of both homogeneity and normality, although not generally applicable for the description of initial imperfections of shells, is adopted in this study and elsewhere [13,15,21] for simplicity and due to the fact that there is no experimental data available for this type of cylindrical panels.

The radius of the structure is treated as random parameter of the imperfect geometry and is modelled with a 2D-1V homogeneous stochastic field fluctuating around its perfect geometry:

$$r(x, y) = r_0 + f_1(x, y)h \tag{1}$$

where r_0 is the radius of the perfect geometry, $f_1(x, y)$ is a zero mean Gaussian homogeneous stochastic field and h is the height of the cylindrical panel. In the present paper the amplitude of the imperfections, which is controlled by the standard deviation of the stochastic field, is selected to be a percentage of the height h of the cylindrical panel. The coordinates x, y are the global Cartesian coordinates of the

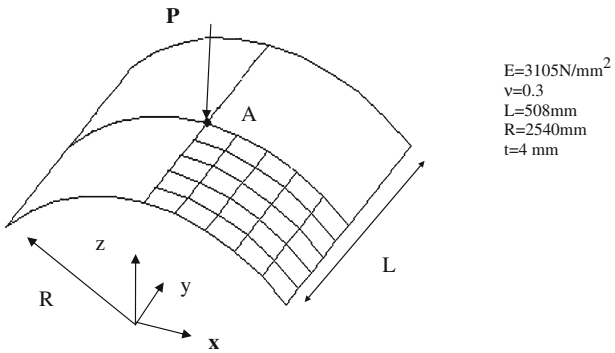

Fig. 1 Example 1: geometry and material data of the cylindrical panel

unfolded panel. A two-sided power spectral density function is used for the description of stochastic field $f_1(x, y)$ which is assumed to correspond to an autocorrelation function of exponential type and is given by

$$S_{f_0 f_0}(\kappa_1, \kappa_2) = \frac{\sigma_f^2}{4\pi} b_1 b_2 \exp\left[-\frac{1}{4}(b_1^2\kappa_1^2 + b_2^2\kappa_2^2)\right] \quad (2)$$

where σ_f denotes the standard deviation of the stochastic field and b_1, b_2 denote the parameters that influence the shape of the spectrum which are proportional to the correlation distances of the stochastic field along the x_1, x_2 axes, respectively.

Moreover, the shape of the imperfections is controlled by the correlation lengths of the stochastic field $f_1(x, y)$. These correlation lengths are usually derived from experimental data and play a significant role on the buckling behaviour of shells [13–15,17]. Since no experimental data is available for this type of problems, a parametric study was performed in [14] with respect to the correlation lengths of the stochastic field in both x, y directions. The outcome of this parametric study produced the "worst" imperfection mode of the shell which leads to the estimation of the lower bound of the buckling load of the shell.

2.2 Imperfect geometry of the axially compressed cylinder

Initial geometric imperfections of the axially compressed cylinder of Fig. 8 are modeled as a two-dimensional non-homogeneous stochastic field. The mean material and geometric properties of the perfect cylinder are also shown in Fig. 8. Following a procedure similar to the one used in [14], the mean values as well as the evolutionary power spectra of the aforementioned non-homogeneous fields are derived from corresponding experimental measurements [22].

The imperfect geometry of the shell is represented by the spatial variation of the radius of the structure as follows:

$$r(x, y) = R + a_0(x, y) + f_1(x, y) \quad (3)$$

where R is the radius of the perfect cylinder, $a_0(x, y)$ is the mean function of the imperfections with respect to the perfect geometry of the shell and $f_1(x, y)$ is a zero-mean non-homogeneous Gaussian stochastic field.

The mean function $a_0(x, y)$ as well as the properties of stochastic field $f_1(x, y)$ are derived from a statistical analysis of experimentally measured imperfections on seven copper electroplated cylindrical shells, named as A shells, taken from a data bank of initial imperfections [22]. For the description of the non-homogeneous field $f_1(x, y)$ in Eq. (3), an evolutionary form of the spectral representation method is implemented [14,23,24]. The evolutionary power spectrum adopted in the present study is assumed to be uncoupled with respect to the axial and circumferential directions of the cylinder, since this is implied by the experimental measurements [14,17]. Therefore, the evolutionary power spectrum used for modeling the stochastic field $f_1(x, y)$ can be written in the following form:

$$S^E(\kappa_x, \kappa_y, x, y) = S_x^E(\kappa_x, x) S_y^E(\kappa_y, y) \quad (4)$$

where $S_x^E(\kappa_x, x)$ and $S_y^E(\kappa_y, y)$ are two independent one-dimensional power spectra for the axial and circumferential direction, respectively. These power spectra were obtained using a windows type sampling procedure. A detailed description of this procedure can be found in [14].

3 Stochastic stiffness matrix

The finite element analysis is performed using the TRIC triangular shell element, which is based on the natural mode method developed by Argyris. The TRIC shear-deformable facet shell element is a reliable and cost-effective element suitable for linear and nonlinear analysis of thin and moderately thick isotropic as well as composite plate and shell structures. The element has 18 degrees of freedom (6 per node) and hence 12 natural straining modes. Three natural axial strains and natural transverse shear strains are measured parallel to the edges of the triangular element. The natural stiffness matrix is derived from the statement of variation of the strain energy with respect to the natural coordinates [25,26].

The modulus of elasticity as well as the thickness of the structure are also considered in the present study as "imperfections" due to their spatial variability. Therefore, these parameters are also described by two independent 2D-1V homogeneous stochastic fields

$$\mathrm{E}(x, y) = E_0 [1 + f_2(x, y)] \quad (5)$$

$$t(x, y) = t_0 [1 + f_3(x, y)] \quad (6)$$

where E_0 is the mean value of the elastic modulus, t_0 is the mean thickness of the structure and $f_2(x, y)$, $f_3(x, y)$ are two zero mean Gaussian homogeneous stochastic fields corresponding to the variability of the modulus of elasticity and the thickness of the shell, respectively. The stochastic stiffness matrix of the shell element is derived using the midpoint method, i.e., a single random variable is assigned for the modulus of elasticity and the thickness of the shell generated from Eqs. (5) and (6), respectively, using the coordinates of the element's centroid [27]. A large number $\mathrm{N_{SAMP}}$ of sample functions are produced leading to the generation of a set of stochastic stiffness matrices incorporating the geometric material and thickness spatially variability. For each set of the aforementioned matrices the buckling load is estimated using the proposed linearized buckling methodology and, for comparison reasons, a full geometric nonlinear analysis

using the arc-length path-following technique. The first and second order moments as well as histograms of the computed sample set of buckling loads are obtained from a statistical analysis of the computed results.

4 Nonlinear analysis

The geometric stiffness of the TRIC shell element consists of two parts: The rigid body contribution and the natural mode contribution. A simplified geometric stiffness matrix is generated by the rigid-body movements of the element and a natural geometric stiffness matrix is computed due to the coupling between the axial forces and the symmetric bending modes. To construct the geometric stiffness, small rigid-body rotational increments about the local Cartesian axes are considered. These rigid-body rotational increments correspond to nodal Cartesian moments along the same axes. In addition to the geometric stiffness corresponding to the rigid-body movements of the element, an approximate natural geometric stiffness, arising from the coupling between the axial forces and the symmetric bending mode (stiffening or softening effect), is also considered. A full description of the linear elastic and geometric stiffness matrix of the TRIC shell element can be found in [25,26].

The solution of the nonlinear system of equations at each Monte Carlo Simulation can be performed using standard incremental-iterative continuation schemes such as the Newton Raphson algorithm in conjunction with the arc-length path-following technique. Such a procedure enables the prediction of the full nonlinear pre and post buckling load-displacement path [14,17]. Alternatively, the bucking load of the structure can be efficiently approximated using the linearized buckling method [28]. This method is based on the assumption that the tangent stiffness matrix varies linearly between two adjacent load increments leading to a partial eigenvalue problem that has to be solved at each MCS.

4.1 Linearized buckling eigensystems

MCS-based linearized buckling analysis of structures with stochastic properties requires the solution of successive eigenproblems, since the stiffness matrices involved change in every simulation and every load increment. In particular, each simulation i $(i = 1, \ldots, n_{\text{sim}})$ requires the solution of eigenproblems of the form:

$$ {}^{t-\Delta t}\mathbf{K}_i\,\boldsymbol{\varphi}_i = \lambda({}^{t-\Delta t}\mathbf{K}_i - {}^{t}\mathbf{K}_i)\boldsymbol{\varphi}_i \tag{7} $$

or equivalently,

$$ {}^{t}\mathbf{K}_i\,\boldsymbol{\varphi}_i = \gamma_i\,{}^{t-\Delta t}\mathbf{K}_i\,\boldsymbol{\varphi}_i, \quad \gamma = \frac{\lambda - 1}{\lambda} \tag{8} $$

where ${}^{t}\mathbf{K}_i$, ${}^{t-\Delta t}\mathbf{K}_i$ are the stiffness matrices associated with the i-th simulation at analysis steps t and $t-\Delta t$, respectively. Then the buckling load can be obtained after solving the corresponding partial eigenvalue problem, as follows:

$$ \mathrm{P}_i^u = {}^{t-\Delta t}\mathrm{P}_i + \lambda_{\min}({}^{t}\mathrm{P} - {}^{t-\Delta t}\mathrm{P}) \tag{9} $$

where ${}^{t}\mathrm{P}_i$, ${}^{t-\Delta t}\mathrm{P}_i$ are the load increments at analysis steps t and $t-\Delta t$, respectively, associated with the i-th simulation and $\lambda_{\min}$ is the lowest eigenvalue of the system.

Now let $\mathbf{K}_0$ be the linear stiffness matrix of the perfect structure. Then, equation (8) can be written as:

$$ \left(\mathbf{K}_0 + {}^{t}\Delta\mathbf{K}_i\right)\boldsymbol{\varphi}_i = \gamma_i\,{}^{t-\Delta t}\mathbf{K}_i\,\boldsymbol{\varphi}_i, \tag{10} $$

which specifies a set of reanalysis-type or nearby eigenproblems. Matrix ${}^{t}\Delta\mathbf{K}_i$, which defines the difference between the stiffness matrices $\mathbf{K}_0$ and ${}^{t}\mathbf{K}_i$, is generally small compared to $\mathbf{K}_0$.

Several solution procedures have been proposed for solving the series of the eigensystems of the form given in (8) or (10). Analytic and semi-analytic solutions that have been proposed are not generally applicable and are restricted by assumptions regarding the probability density function of the results [29,31]. In addition, Galerkin-based solutions in the context of the polynomial chaos expansion method have been successfully applied for treating the random eigenvalue problem, however, they are mainly formulated for spatial variations of the random system properties, while the problem of random geometric imperfections is not addressed [30]. On the other hand, Monte Carlo simulation based numerical solutions are generally applicable and have been applied in similar problems together with subspace iteration schemes in conjunction with the mode component mode synthesis method, in order to reduce the enormous computational cost involved in the MCS [31]. The aforementioned methods are basically applied in dynamic systems where a large number of eigenvectors have to be computed.

In our case however, only the smallest eigenvalue of the linearized buckling eigensystem is required. For this reason, an alternative eigensolution scheme based on the Preconditioned Conjugate Gradient (PCG) method is applied in this work for the computation of the smallest eigenvalue and corresponding eigenvector of a stochastic eigensystem. This eigensolution scheme can handle the type of eigenproblems encountered in linearized buckling analysis in a computationally efficient way.

4.2 The EIGPCG solution method

The EIGPCG method is an efficient iterative procedure for solving large-scale sparse eigensystems, when only limited number of eigenvalues is required [32,33]. Given a generalized eigenvalue problem of the form

$$\mathbf{Ax} = \lambda \mathbf{Bx}, \tag{11}$$

where $\mathbf{A}$, $\mathbf{B}$ are $n \times n$ symmetric matrices, $\mathbf{x}$ is the eigenvector and λ is the eigenvalue, the EIGPCG algorithm aims at minimizing the Rayleigh quotient (R-Q):

$$f(\mathbf{x}) = \frac{\mathbf{x}^t \mathbf{Ax}}{\mathbf{x}^t \mathbf{Bx}}. \tag{12}$$

$f(\mathbf{x})$ is stationery and equal to an eigenvalue when $\mathbf{x}$ is the corresponding eigenvector. Thus, by minimizing the R-Q of Eq. (12), the smallest eigenvalue is obtained along with the corresponding eigenvector. R-Q minimization is performed in this work with the EIGPCG algorithm, which is based on the standard PCG procedure and proceeds as follows:

Initialization

$$\mathbf{x}^{(0)} = \mathbf{1}$$
$$f^{(0)} = \frac{\mathbf{x}^{(0)t} \mathbf{Ax}^{(0)}}{\mathbf{x}^{(0)t} \mathbf{Bx}^{(0)}}$$
$$\mathbf{g}^{(0)} = \frac{2}{\mathbf{x}^{(0)t} \mathbf{Bx}^{(0)}} \left(\mathbf{Ax}^{(0)} - f^{(0)} \mathbf{Bx}^{(0)} \right)$$
$$\mathbf{z}^{(0)} = \tilde{\mathbf{A}}^{-1} \mathbf{g}^{(0)} \quad \text{(preconditioning step)}$$
$$\mathbf{p}^{(0)} = \mathbf{z}^{(0)}$$

Iterations $m = 1, 2, \ldots$, *(until convergence)*

Calculate the solution $\alpha^{(m-1)}$ of trinomial equation $u^{(m-1)} \alpha^{(m-1)^2} + v^{(m-1)} \alpha^{(m-1)} + w^{(m-1)} = 0$ with:

$$u^{(m-1)} = \left(\mathbf{p}^{(m-1)t} \mathbf{Ap}^{(m-1)} \right) \left(\mathbf{x}^{(m-1)t} \mathbf{Bp}^{(m-1)} \right) - \left(\mathbf{x}^{(m-1)t} \mathbf{Ap}^{(m-1)} \right) \left(\mathbf{p}^{(m-1)t} \mathbf{Bp}^{(m-1)} \right)$$
$$v^{(m-1)} = \left(\mathbf{p}^{(m-1)t} \mathbf{Ap}^{(m-1)} \right) \left(\mathbf{x}^{(m-1)t} \mathbf{Bx}^{(m-1)} \right) - \left(\mathbf{x}^{(m-1)t} \mathbf{Ax}^{(m-1)} \right) \left(\mathbf{p}^{(m-1)t} \mathbf{Bp}^{(m-1)} \right)$$
$$w^{(m-1)} = \left(\mathbf{x}^{(m-1)t} \mathbf{Ap}^{(m-1)} \right) \left(\mathbf{x}^{(m-1)t} \mathbf{Bx}^{(m-1)} \right) - \left(\mathbf{x}^{(m-1)t} \mathbf{Ax}^{(m-1)} \right) \left(\mathbf{x}^{(m-1)t} \mathbf{Bp}^{(m-1)} \right)$$
$$\mathbf{x}^{(m)} = \mathbf{x}^{(m-1)} + \alpha^{(m-1)} \mathbf{p}^{(m-1)}$$
$$vf^{(m)} = \frac{\mathbf{x}^{(m)t} \mathbf{Ax}^{(m)}}{\mathbf{x}^{(m)t} \mathbf{Bx}^{(m)}}$$
$$\text{IF } \left| \frac{f^{(m)} - f^{(m-1)}}{f^{(m-1)}} \right| \leq \varepsilon \text{ STOP} \quad \text{(convergence check)}$$
$$\mathbf{g}^{(m)} = \frac{2}{\mathbf{x}^{(m)t} \mathbf{Bx}^{(m)}} \left(\mathbf{Ax}^{(m)} - f^{(m)} \mathbf{Bx}^{(m)} \right)$$
$$\mathbf{z}^{(m)} = \tilde{\mathbf{A}}^{-1} \mathbf{g}^{(m)} \quad \text{(preconditioning step)}$$
$$\beta^{(m)} = \frac{\mathbf{g}^{(m)t} \mathbf{z}^{(m)}}{\mathbf{g}^{(m-1)t} \mathbf{z}^{(m-1)}}$$
$$\mathbf{p}^{(m)} = \mathbf{z}^{(m)} + \beta^{(m)} \mathbf{p}^{(m-1)}$$

In the above algorithm ε is a user defined tolerance controlling the solution accuracy obtained for the eigenvalue f, while $\tilde{\mathbf{A}}$ represents the preconditioning matrix.

Applying an appropriate preconditioning matrix to accelerate convergence plays a crucial role in the success of any PCG method, especially for ill-conditioned problems. The preconditioning matrix $\tilde{\mathbf{A}}$ in the above algorithm is intended to be an approximation to $\mathbf{A}$ and has to be selected in a way that the eigenvalues of $\tilde{\mathbf{A}}^{-1}\mathbf{A}$ are spread as uniformly as possible over a much narrower spectrum than those of $\mathbf{A}$. Among several options available to precondition a conjugate gradient procedure, incomplete Cholesky factorization has been shown to be an effective and efficient preconditioning technique that can drastically increase the convergence rate at the expense of some additional storage requirements.

The iterative nature of the EIGPCG method allows the adaptation of this solution scheme to the special features of nearby eigenproblems encountered in linearized buckling reanalyses. For each simulation i and analysis step t an eigensolution of a system of the form in Eq. (11) (with $\mathbf{A} = {}^t\mathbf{K}_i$, $\mathbf{B} = {}^{t-\Delta t}\mathbf{K}_i$) needs to be solved. EIGPCG can be customized to take into account the relatively small differences between stiffness matrices ${}^t\mathbf{K}_i$ for different i, thus avoiding the solution of the systems in Eq. (8) as stand-alone eigenproblem. The customized EIGPCG procedure for the solution of stochastic eigenvalue problems in the framework of a linearized buckling analysis makes use of an efficient preconditioning technique employed to accelerate its convergence during the successive eigensolutions. The EIGPCG-$\mathbf{K}_0$ solution method described below, which is a specialized version of the EIGPCG algorithm, utilizes a preconditioner in the form of $\mathbf{K}_0$ combined with proper matrix handling schemes, under the assumption that the matrix terms contained in ${}^t\Delta\mathbf{K}_i$ are small compared to those in $\mathbf{K}_0$.

4.3 The EIGPCG-$\mathbf{K}_0$ solution method

Reanalysis type eigenproblems of the form given in Eq. (10) can be effectively solved using the EIGPCG algorithm equipped with a preconditioner following the rationale of incomplete Cholesky preconditionings [34,35]. The incomplete factorization of the stiffness matrix $\mathbf{K}_0 + {}^t\Delta\mathbf{K}_i$ can be written as:

$${}^t\tilde{\mathbf{L}}_i^t {}^t\tilde{\mathbf{D}}_i^t {}^t\tilde{\mathbf{L}}_i^t = \mathbf{K}_0 + {}^t\Delta\mathbf{K}_i - {}^t\mathbf{E}_i, \tag{13}$$

where ${}^t\tilde{\mathbf{D}}_i$ is a diagonal matrix, ${}^t\tilde{\mathbf{L}}_i$ is a lower triangular matrix with unit elements on the leading diagonal and ${}^t\mathbf{E}_i$ is an error matrix which does not have to be formed. Matrix ${}^t\mathbf{E}_i$ is defined either by the magnitude of "small" elements

in ${}^t\tilde{\mathbf{L}}_i$ which do not satisfy a specified magnitude criterion and therefore are discarded or by a specified topology of ${}^t\tilde{\mathbf{L}}_i$ which usually conforms with the sparsity features of $\mathbf{K}_0$. For the typical reanalysis eigenproblem of Eq. (10) matrix ${}^t\mathbf{E}_i$ is taken as ${}^t\Delta\mathbf{K}_i$ and the preconditioning matrix becomes the complete factorized initial stiffness matrix: $\tilde{A} = K_0$. If matrix ${}^t\Delta\mathbf{K}_i$ is sufficiently small compared to $\mathbf{K}_0$, we can expect that $\tilde{A} = K_0$ will act as a strong preconditioner for the successive conjugate gradient eigensolutions. The EIGPCG algorithm equipped with the preconditioner $\tilde{A} = K_0$ throughout the entire linearized buckling analysis and simulation process constitutes the EIGPCG-$\mathbf{K}_0$ method for the solution of the nearby eigenproblems of Eq. (10).

With preconditioning matrix $\tilde{A} = K_0$ remaining the same during the successive eigenvalue reanalyses, the repeated solutions required for the preconditioning step of the EIGPCG algorithm can be treated as problems with multiple right-hand sides:

$$\tilde{\mathbf{A}}\,{}^t\mathbf{z}_i^{(m)} = {}^t\,\mathbf{g}_i^{(m)}, \tag{14}$$

since the entries in the vector $\mathbf{g}$ are updated at each EIGPCG iteration m of simulation i and load increment t. Therefore, the linear stiffness matrix of the perfect structure $\mathbf{K}_0$ is retained in factorized form (using a skyline storage scheme) throughout all simulations and analysis steps. Hence, the solution of the preconditioning step in Eq. (14), which has to be performed at each EIGPCG iteration of all simulations and analysis steps, can be effortlessly executed—once $\mathbf{K}_0$ is factorized, by a forward substitution, a vector operation and a backward substitution. In other words, the EIGPCG preconditioning step is handled with a direct solution scheme, which is capable of solving problems with multiple right-hand sides very efficiently.

It is pointed out that EIGPCG-$\mathbf{K}_0$ retains in memory its factorized preconditioner $\mathbf{K}_0$ throughout the whole analysis and simulation process using single precision arithmetic for floating point information. On the other hand, double precision storage is required for all floating point stiffness data associated with stiffness matrices ${}^t\mathbf{K}_i$, which are stored using a compact storage scheme (only the non-zero terms of each matrix are retained in memory together with addresses indicating the position of each stored term in the matrix).

5 Numerical examples

Example 1 The hinged isotropic cylindrical panel of Fig. 1, with a considerable nonlinear behaviour before its limit point, is selected in order to illustrate the efficiency of the proposed linearized buckling methodology. The loading as well as the geometric and material properties of the perfect shell are also shown in Fig. 1. The curve edge nodes of the panel are assumed to be free in all directions while the nodes along the sides are hinged (fixed against translation). The material is considered to be elastic. The geometrically nonlinear elastic response of point A of the perfect cylinder with respect to the applied vertical load P is shown in Fig. 2, where the cylindrical panel is discretized with a mesh of 21×21 nodes and 400 TRIC shell elements. The same mesh is used for the discretization of the stochastic fields since the resulting element size is a fraction of the correlation lengths adopted in this example. The ultimate load of the perfect configuration is found to be $P_u = 203.4$ N.

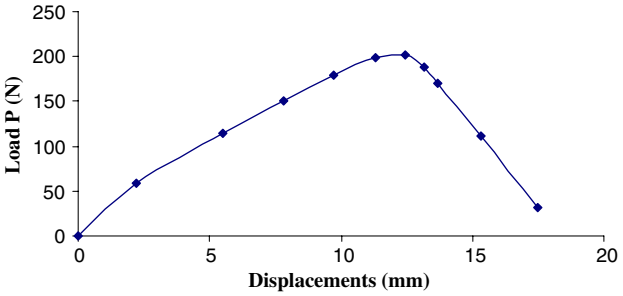

Fig. 2 Example 1: central load-displacement curve of the perfect cylindrical panel

5.1 Initial geometric imperfections

Two-dimensional (2D) stochastic imperfections are introduced to the model in order to investigate their effect on the buckling load of the panel. The thickness of the shell is considered to be $t = 4$ mm. For all cases, the standard deviation σ_f of the stochastic field of the initial geometric imperfections is assumed to be $\sigma_f = 0.02h$, where h is the height at the apex of the cylindrical panel. In order to predict "worst" imperfection modes which lead to the estimation of the lower buckling loads of the shell, a parametric study has to be performed for this problem with respect to the correlation lengths of the stochastic fields in both x, y directions. It is assumed that the correlation lengths in both x and y directions are equal, $b = b_1 = b_2$, since there are no specific manufacturing procedures or boundary conditions that would indicate a different assumption.

The aforementioned sensitivity analysis is carried out using the proposed linearized buckling methodology and a more accurate nonlinear incremental-iterative procedure using the arc-length path-following method. Figure 3a presents the mean value of the buckling loads as a function of the correlation length parameter, obtained using the proposed linearized buckling approach as well as the "exact" path-following technique. Figure 3b presents the corresponding results for the Coefficient of Variation (Cov) of the buckling loads. From these figures it can be observed that the results obtained with the linearized buckling procedure are close to

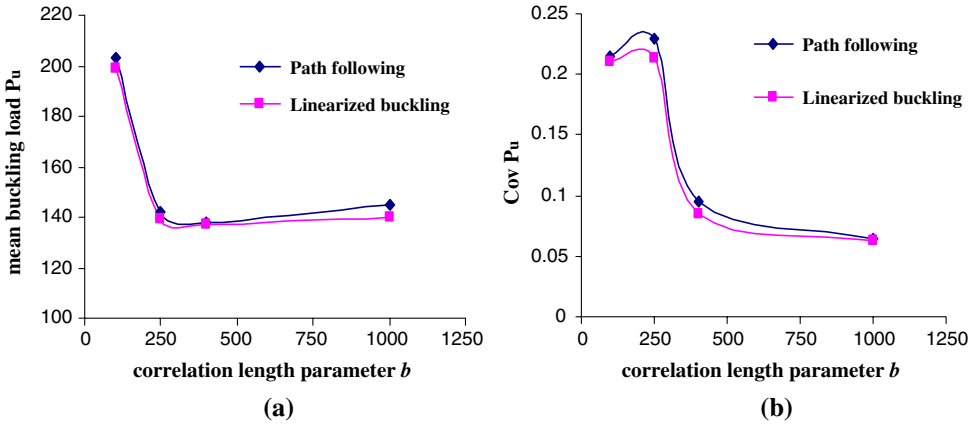

Fig. 3 Example 1: mean value (**a**) and coefficient of variation (**b**) of the ultimate load P_u of the imperfect shell as a function of the correlation length parameter b

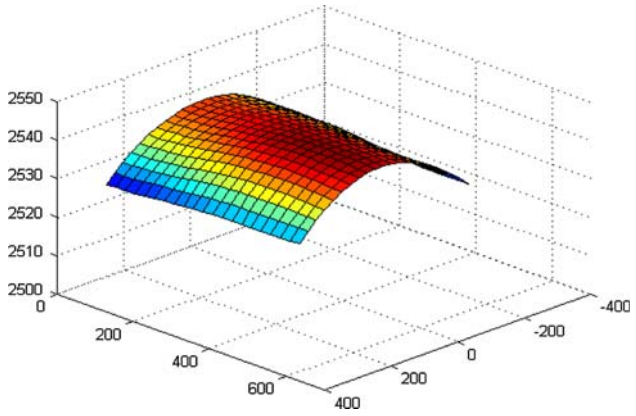

Fig. 4 Example 1: 2D initial imperfection shape for correlation length parameter $b_1 = b_2 = 250$

the corresponding results obtained with the the "exact" path-following analysis. The largest relative error is found to be 3.5 ($b = 1,000$) and 7% ($b = 250$) for the mean value and Cov, respectively. Both approaches predict the same "worst" imperfection mode which corresponds to a correlation length parameter $b = 250$. In Fig. 4 one sample function of initial geometric imperfections generated for the aforementioned correlation parameter is presented.

5.2 Combination 1: initial geometric imperfections and material imperfections

Two-dimensional random material imperfections are combined and introduced simultaneously to the model of the imperfect cylindrical panel. For the initial geometric imperfections the "worst" scenario of $b = 250$ mm, obtained from the previous sensitivity analysis presented in Fig. 3, is used for this combination. The standard deviation for the modulus of elasticity is assumed to be 10% of its mean value. Figure 5a shows the mean value of the buckling loads as a function of the correlation length parameter for the modulus of elasticity obtained using the proposed linearized buckling approach as well as corresponding results obtained using the "exact" path-following technique. Similar results are shown in Fig. 5b for the Cov of the buckling loads. From these figures it can be seen that the results obtained with the linearized buckling procedure are close to the corresponding results obtained with the "exact" path-following analysis. The largest relative error is found to be 3.5 ($b = 2,000$) and 6.5% ($b = 500$) for the mean value and the Cov, respectively, while both approaches predict the same "worst" mode which corresponds to a correlation length parameter $b = 2,000$ for the modulus of elasticity .

5.3 Combination 2: initial geometric, material and thickness imperfections

Two-dimensional random thickness imperfections are now combined and introduced simultaneously to the model of the cylinder with initial geometric and material imperfections. For the initial geometric imperfections the "worst" scenario of $b = 250$, obtained from the initial sensitivity analysis shown in Fig. 3, is also used for this combination, while the value of $b = 2,000$ is adopted for the modulus of elasticity, as was found from the sensitivity analysis of the previous Combination 1. The standard deviation of the thickness is assumed to be 10% of its mean value. Figure 6a depicts the mean value of the buckling loads as a function of the correlation length parameter for the thickness obtained with the proposed linearized buckling approach and the "exact" path-following technique. Figure 6b depicts the corresponding results for the Cov of the buckling loads. It can be observed that the results obtained with the linearized buckling procedure are close to the corresponding results obtained with the "exact" path-following analysis. The largest relative error is found to be 3.5 ($b = 2,000$) and 7% ($b = 500$) for the mean value and the Cov, respectively, while both approaches predict the same "worst" mode which corresponds to a correlation length parameter for the thickness $b = 2,000$.

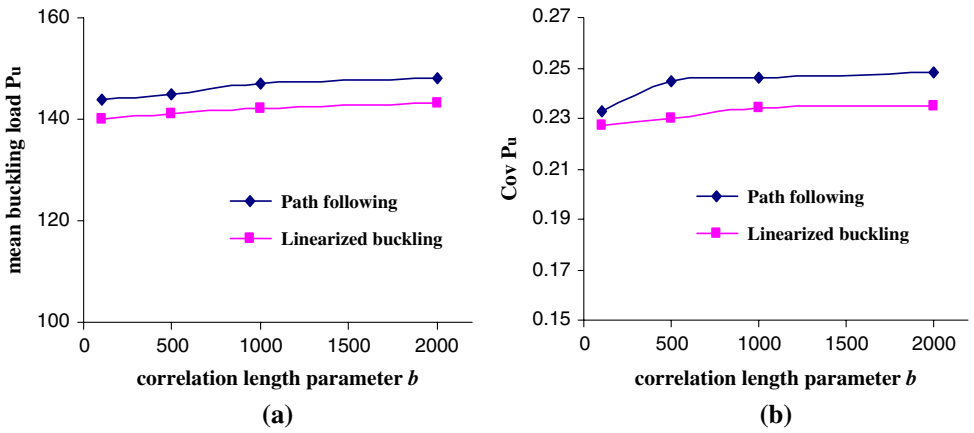

Fig. 5 Example 1: mean value (**a**) and coefficient of variation (**b**) of the ultimate load P_u of the imperfect shell, combined with a 2D variation of the modulus of elasticity, as a function of the correlation length parameter b for the modulus of elasticity

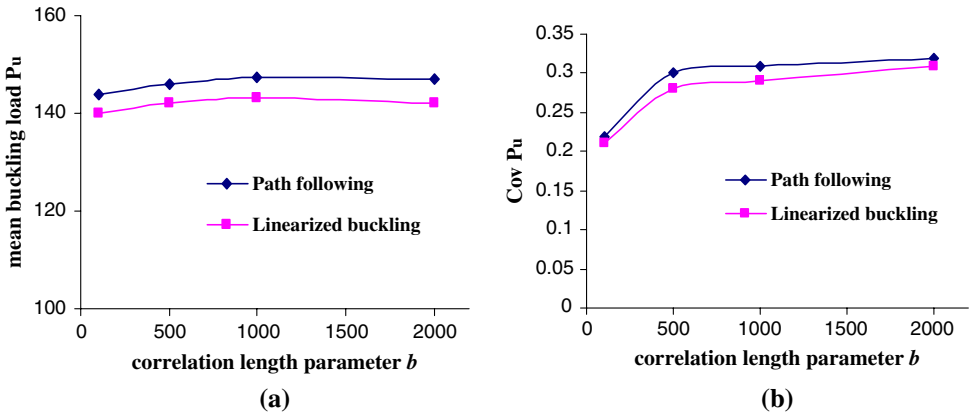

Fig. 6 Example 1: mean value (**a**) and coefficient of variation (**b**) of the ultimate load P_u of the imperfect shell, combined with 2D variations of the modulus of elasticity and thickness, as a function of the correlation length parameter b for the thickness

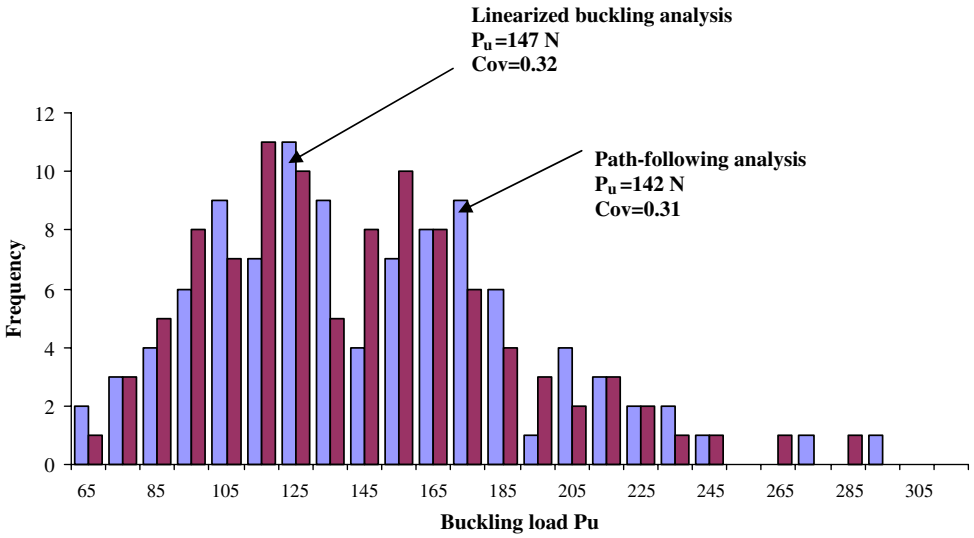

Fig. 7 Example 1: histograms of critical load factors for all 2D combined imperfections using the proposed linearized buckling approach and a path following analysis

Finally, histograms of the buckling loads are computed using both the proposed linearized buckling methodology as well as the standard incremental-iterative nonlinear analysis with the arc-length path-following technique. These histograms are presented in Fig. 7 and correspond to the previously established "worst" case scenario regarding all involved uncertain parameters: $b = 250$ for the initial geometric imperfections and $b = 2{,}000$ for the material and thickness variability. It can observed that the proposed linearized buckling approach leads to accurate predictions of the mean value and Cov of the buckling loads as well as of the shape of the buckling loads distribution and the corresponding minimum and maximum buckling load values.

Example 2 The thin-walled isotropic axially compressed cylinder of Fig. 8 with a limited nonlinear behaviour before

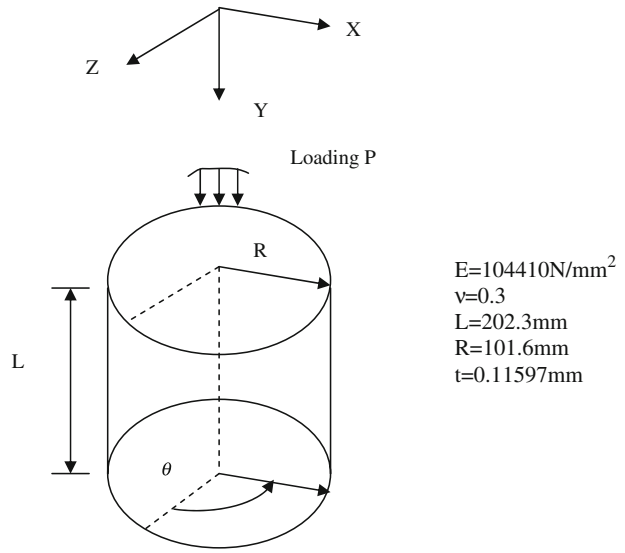

Fig. 8 Example 2: geometry and material data of the axially compressed cylinder

the manifestation of the limit point is selected as the second example. The loading as well as the geometric and material properties of the perfect cylinder are also shown in Fig. 8. The base edge nodes of the cylinder are fixed against all translations, fixed against rotations around the Y axis and free against rotations around the X and Z axis. The top edge nodes of the cylinder are fixed against X and Z translations, fixed against rotations around the Y axis, free against translations in the Y axis and free against rotations around axis X and Z.

For this problem, an extensive investigation was performed in [17], where imperfections were described as two-dimensional non-homogenous stochastic fields with statistical properties that were derived form a data bank of measured imperfections [22]. Extensions to this investigation that include, not only the initial imperfect geometry but also the variability of the modulus of elasticity and the thickness of the cylinder as well as the non-uniformity of the axially applied load was presented in [14] and [16], respectively. In these works extensive investigations were performed with respect to the adequacy of the finite element model to accurately predict the pre-buckling state of deformation as well as critical load factors, through mesh convergence studies as well as through comparisons of the numerically predicted buckling loads with corresponding predictions of bifurcation points using semi-analytic methods based on Koiter's imperfection sensitivity theory [1].

More particular, mesh convergence studies of the imperfect cylinder were computed in [16] for a randomly selected generation of geometric imperfections using Eq. (3). It was shown that a relatively coarse mesh with TRIC shell elements is adequate for the analysis of the imperfect cylinder with respect to the mesh required for the analysis of the perfect one. This is explained by the fact that the buckling modes of the imperfect cylinder are mainly dominated by the imperfections' pattern and not by some higher order modes of the perfect cylinder, which require a more refined disretization with TRIC shell elements in order to be captured by the finite element analysis. Figure 9 presents the results of the aforementioned convergence study. The predicted buckling loads for the various mesh sizes correspond to the load level at which the first negative eigenvalue of the tangent stiffness matrix of the structure appears and are normalized with respect to the theoretical buckling load of the perfect cylinder, given by:

$$P_u^{(\text{perfect})} = \frac{Et^2}{R\sqrt{3(1-\upsilon^2)}} = 5{,}350\ \text{N} \tag{15}$$

From this figure it can be seen that a relatively coarse mesh of 51×101 nodes, produces a very small ($\sim$1%) relative discretization error of the buckling loads with respect to buckling loads calculated with more refined meshes. For the refined mesh of a 51×401, the normalized buckling load was computed at $\lambda_{cr} = 0.857$ resulting in a relative, with respect to the "exact" semi-analytic solution, error of the order of 1.5% [16]. Thus, the mesh of 51×101 nodes is adopted here for the subsequent sensitivity studies. In addition, this mesh provides a sufficiently accurate representation of the gradients of the imperfect shape of the cylinder, since its element size is a fraction of the correlation lengths of the stochastic fields used for both axial and circumferential directions. This can be seen in Fig. 10 where a sample realization of initial geometric imperfections generated by Eq. (3) is presented for this particular mesh size.

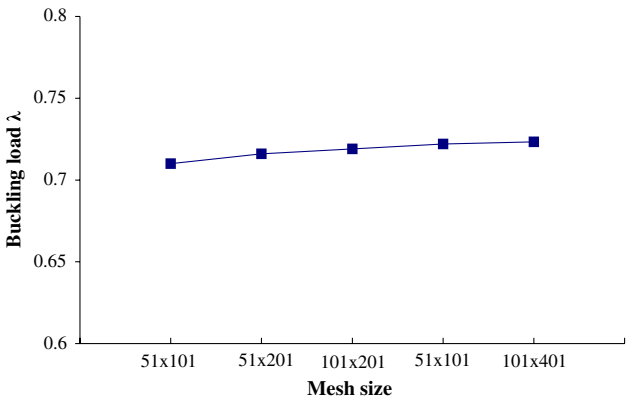

Fig. 9 Example 2: convergence behaviour for a randomly selected MCS simulation of the imperfect cylinder loaded with a non-uniform axial load

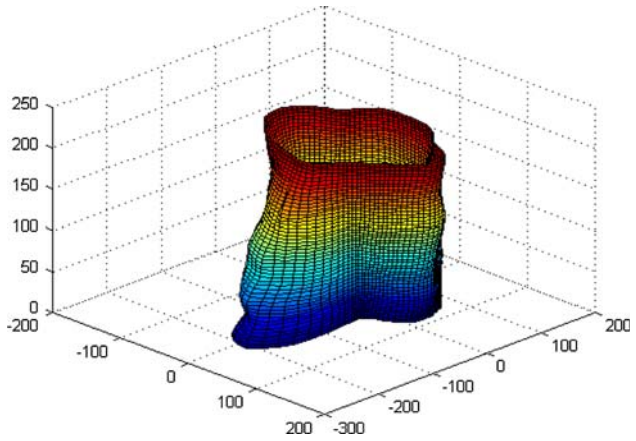

Fig. 10 Example 2: sample realization of non-homogeneous out-of-plane geometric imperfections using evolutionary power spectra and a mesh of 51 × 101 nodes

5.4 Combination 1: initial geometric and material imperfections

Two-dimensional random material imperfections are combined and introduced simultaneously to the model of the imperfect cylinder. For the initial geometric imperfections no sensitivity analysis is required since, as previously mentioned, the evolutionary power spectra of the corresponding stochastic fields are based on a statistical analysis of experimental results [14,22]. The standard deviation of the modulus of elasticity is assumed to be 10% of its mean value. Figure 11a presents the mean value of the buckling loads as a function of the correlation length parameter for the modulus of elasticity obtained using the proposed linearized buckling approach as well as the "exact" path-following technique. Figure 11b presents analogous results for the Cov of the buckling loads. From these figures it can be seen that, as in the previous example, the results obtained with the linearized buckling procedure are close to the corresponding results obtained with the "exact" path-following analysis leading to the same conclusion that small correlation lengths ($b = 50$) are responsible for the lowest mean value of the buckling loads, while large correlation lengths ($b = 500$) result in higher values of the Cov. The largest relative error is found to be 5.5 ($b = 50$) and 15% ($b = 100$) for the mean value and the Cov, respectively.

5.5 Combination 2: initial geometric, material and thickness imperfections

Two-dimensional random thickness imperfections are now combined and introduced simultaneously to the model of the cylinder with initial geometric and material imperfections. The standard deviation of the thickness is assumed to be 10% of its mean value. Figure 12a presents the mean value of the buckling loads as a function of the correlation length parameter for the thickness obtained with the proposed linearized buckling approach and the "exact" path-following technique, while Fig. 12b presents similar results for the Cov. As in the previous Combination, both approaches confirm the conclusion that a correlation length of $b = 50$ is responsible for the lowest mean value of the buckling loads, while a correlation lengths of $b = 500$ results in higher values of the Cov. The largest relative error is found to be 5.5 ($b = 500$) and 15% ($b = 50$) for the mean value and the Cov, respectively.

Finally, histograms of the buckling loads are presented in Fig. 13 for both the proposed linearized buckling methodology as well as the standard incremental-iterative nonlinear analysis. These histograms are computed for the previously established "worst" case scenario of the lowest mean value $b = 50$ for the material and thickness variability. It can be observed that for this type of shell structures, the proposed linearized buckling methodology also leads to accurate predictions of the mean value and Cov of the buckling loads as well as of the shape of the buckling loads distribution and the corresponding minimum and maximum buckling load values.

5.6 Accuracy of the buckling load prediction

Whether a linearized buckling approach or a nonlinear incremental-iterative analysis is used, it is well known that the accuracy of the prediction of the buckling load is problem

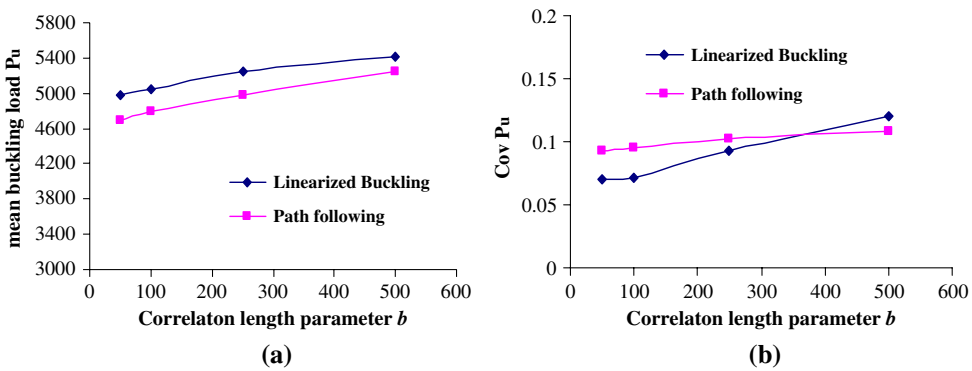

Fig. 11 Example 2: mean value (**a**) and coefficient of variation (**b**) of the ultimate load P_u of the imperfect cylinder, combined with a 2D variation of the modulus of elasticity, as a function of the correlation length parameter b for the modulus of elasticity

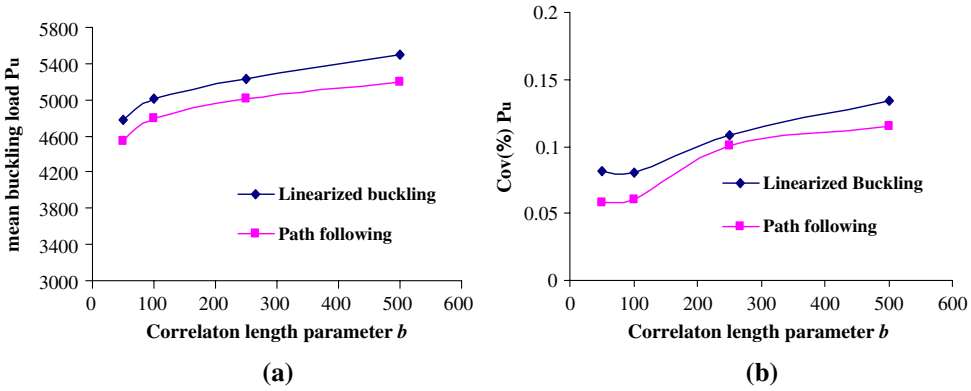

Fig. 12 Example 2: mean value (**a**) and coefficient of variation (**a**) of the ultimate load P_u of the imperfect cylinder, combined with 2D variations of the modulus of elasticity and thickness, as a function of the correlation length parameter b for the thickness

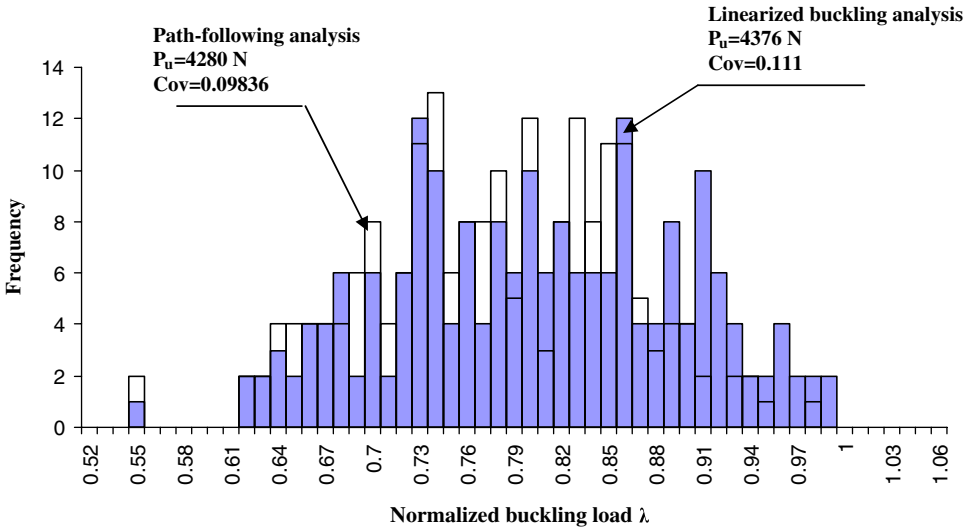

Fig. 13 Example 2: histograms of critical load factors for all 2D combined imperfections using the proposed linearized buckling approach and a path-following analysis

dependent and is affected mainly by the selection of the corresponding load increments. The accuracy of the linearized buckling prediction strongly depends on the positions of the corresponding tangent stiffness matrices of Eq. (8) along the load displacement curves. The closer these stiffness matrices are to the limit point the better prediction of the linearized buckling load is achieved. Thus, the accuracy of the linearized buckling prediction is more sensitive in shell-type structures which exhibit a limit point buckling with large pre-buckling deformation response. In such cases, a two-step analysis procedure is preferable in order to predict the buckling load with an acceptable accuracy. This two-step analysis procedure performs two load increments instead of one in connection to Eq. (8) with $t = 2$. In such cases it appears that the larger the first load increment is taken, the more accurate load predictions are obtained. This is not the case in imperfection-sensitive types of shells, like the axially compressed cylinder of Fig. 8, in which the structural behaviour prior to buckling is almost linear. In such cases the tangent stiffness is almost independent of the level of the first load increment, thus a one-step linearized buckling analysis ($t = 1$ in Eq. (8)) can be implemented.

On the other hand, for nonlinear incremental-iterative analysis, higher accuracy is achieved on the computation of the buckling load with small load increments. Since the selection of very small increments results in an increase in the computational effort, the selection of an appropriate load increment is usually a trade-off between accuracy and efficiency. However, as the small load increments are required only in the neighborhood of the buckling load, a relatively large first load increment can be used in order to avoid unnecessary load increments away from the limit point. The first load increment must be lower than the lowest buckling load of the MCS. Such a selection is not obvious, since this lowest buckling load is unknown a-priori. In the present study, this first load increment is selected to be a fraction of the buckling load of the perfect structure.

The aforementioned considerations can be visualized in Figs. 14 and 15 where the fluctuations of the computed buckling loads at five randomly selected Monte Carlo simulation runs are presented for the cylindrical panel and the axially

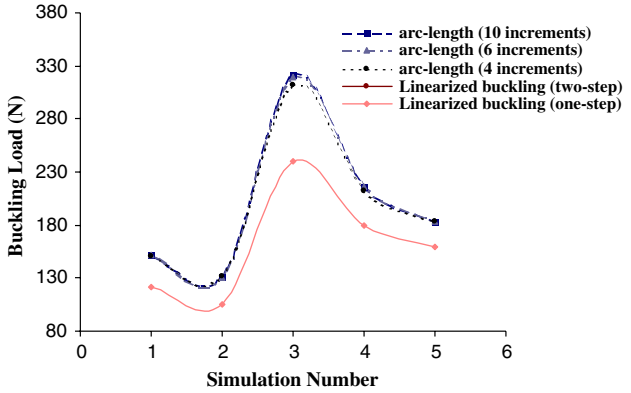

Fig. 14 Example 1: buckling load predictions for five MCS runs using the non-linear incremental-iterative procedure and the linearized buckling approach

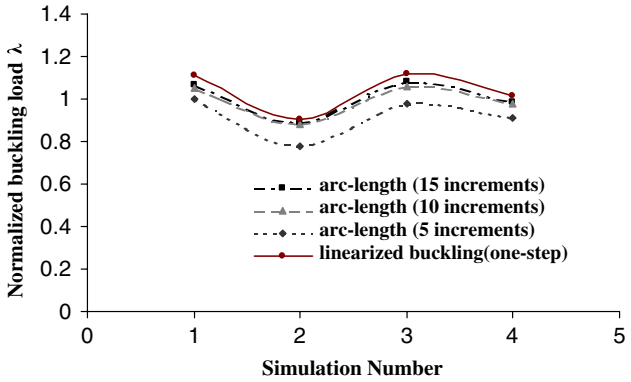

Fig. 15 Example 2: buckling load predictions for five MCS runs using the non-linear incremental-iterative procedure and the linearized buckling approach

compressed cylinder, respectively. Figure 14 presents the sensitivity of the buckling load predictions for the first test example, using the linearized buckling approach and the incremental-iterative nonlinear analysis with various load increments. From this figure it can be observed that the use of a two-step linearized buckling analysis leads to a considerable improvement of the prediction of the buckling loads with respect to the one-step analysis. The accuracy of this procedure is higher compared to the incremental-iterative nonlinear analysis with an average of four increments and is almost the same with the incremental-iterative nonlinear analysis with an average of 6 nonlinear increments up to the limit point. In addition, the buckling load predictions of the linearized buckling procedure are very close to the "exact" values obtained with the nonlinear analysis with an average of 10 load increments .

Figure 15 presents similar results for the axially compressed cylinder. From this example it can be observed that the use of a one-step linearized buckling analysis leads to very good predictions of the buckling loads. The accuracy of this procedure is much higher compared to the incremental-iterative nonlinear analysis with an average of five increments up to the limit point and is almost the same with the incremental-iterative nonlinear analysis with an average of 10 load increments. Furthermore, the buckling load predictions with the linearized buckling procedure are very close to the nonlinear analysis with an average of 16 nonlinear increments which can be considered as "exact". For the aforementioned nonlinear analysis, the first load step is selected to be 60% of the buckling load of the perfect structure.

5.7 Performance of EIGPCG-K_0

The computational performance of the EIGPCG-$\mathbf{K}_0$ solver is presented in Table 1 for the axially compressed cylinder. A sensitivity analysis procedure for this example requires the performance of eight MCS and therefore 800 nonlinear analyses in total. From this Table it can be seen that the computed time required for the aforementioned sensitivity analysis using the proposed linearized buckling methodology is approximately 40 CPU seconds, while if this analysis was performed using an "exact" nonlinear analysis with the modified Newton Raphson (mNR) scheme together with the

Table 1 Example 2: Performance of EIGPCG-$\mathbf{K}_0$ for eight MCS resulting in 800 nonlinear analyses

Method	mNR-arc length	Linearized buckling EIGPCG-K_0
Number of non-linear increments	16.000	1,600
Number of non-linear iterations	35.000	–
Number of CG iterations	–	5,000
Factorization time (s)	970	
Preconditioning time (s)	–	1
Substitutions time (s)	30	–
CG iterations time (s)	–	39
Total time (s)	1,000	40

arc-length path-following technique and an average of 10 nonlinear increments per analysis, would require 1,000 CPU seconds to be performed. Therefore, a drastic reduction of almost two orders of magnitude is achieved, which makes the implementation of such sensitivity analyses in real-world structures tractable. All computing times presented in Table 1 were obtained in a Core 2 Duo Pentium (2,660 MHz).

6 Conclusions

In the present paper an accurate and computationally efficient method is presented for the buckling analysis of shells with random imperfections. The proposed methodology is based on a linearized buckling approximation of the limit load of the shell in the context of a brute-force Monte Carlo Simulation (MCS) used for the overall estimation of the scatter of the buckling loads. The corresponding eigenproblem is solved at each MCS using a variant of the Preconditioned Conjugate Gradient method based on the Rayleigh quotient. The proposed methodology is particularly suitable for cases where lack of experimental data does not allow for a rational and reliable description of the statistical properties of the random fields required for modeling the uncertain parameters. In such cases a computationally expensive sensitivity analysis with respect to assumed parameters, necessary for the description of the stochastic fields, is required, leading to parametric investigations as well as to the identification of "worst case" scenarios with respect to selected response quantities. The numerical results presented demonstrate the advantages of the proposed approach by drastically reducing the computational effort involved in the repeated MCS required for the parametric investigations, compared to the "exact" incremental-iterative nonlinear analysis. This is achieved without sacrificing the accuracy of the buckling load prediction, thus allowing the application of stochastic sensitivity analyses in real-world structures.

References

1. Koiter WT (1963) The effect of axisymmetric imperfections on the buckling of cylindrical shells under axial compression. Prc Koninkl Nederl Akademie van Wetenschappen 66(B):265–279
2. Arbocz J, Babcock CD Jr (1969) The effect of general imperfections on the buckling of cylindrical shells. J Appl Mech 36(1): 28–38
3. Hoff NJ, Soong TC (1969) Buckling of axially compressed circular shells with non-uniform boundary conditions. In: Proc symposium on thin-walled structures their design and use in building, University College of Swansea, pp 61–80
4. Libai A, Durban D (1977) Buckling of cylindrical shells subjected to non-uniform axial loads. ASME paper WA/APM-12
5. Palassopoulos GV (1977) Buckling analysis and design of imperfection sensitive structures. In: Haldar A, Guran BM, Ayyub (eds) Uncertainty modeling in finite element, fatigue and stability of systems, vol 9. World Scientific publishing Company, Singapore, Series on stability, Vibration and Control of System Series B, pp 311–356
6. Li YW, Elishakoff I, Starnes JH Jr, Bushnell D (1997) Effect of the thickness variation and initial imperfection on buckling of composite shells: asymptotic analysis and numerical results by BOSOR4 and PANDA2. Int J Solids Struct 34: 3755–3767
7. Li LY (1990) Influence of loading imperfections on the stability of an axial compressed cylindrical shell. Thin Walled Struct 10: 215–220
8. Greenberg JB, Stavsky Y (1995) Buckling of composite orthotropic cylindrical shells under non-uniform axial loads. Composite Struct 30:399–406
9. Arbocz J (2000) The effect of imperfect boundary conditions on the collapse behaviour of anisotropic shells. Int J Solids Struct 37:6891–6915
10. Arbocz J, Starnes JH Jr (2002) Future directions and challenges in shell stability analysis. Thin Walled Struct 40:729–754
11. Elishakoff I (2000) Uncertain buckling: its past, present and future. Int J of Solids Struct 37:6869–6889
12. Elishakoff I, Li YW, Starnes JH Jr (2001) Nonclassical problems in the theory of elastic stability, XVI. Cambridge University Press, Cambridge, p 336
13. Papadopoulos V, Papadrakakis M (2004) Finite element analysis of cylindrical panels with random initial imperfections. J Eng Mech ASCE 130(8):867–876
14. Papadopoulos V, Papadrakakis M (2005) The effect of material and thickness imperfections on the buckling load of shells with random initial imperfections. Comput Methods Appl Mech Eng 194(12–16):1405–1426
15. Stefanou G, Papadrakakis M (2004) Stochastic finite element analysis of shells with combined random material and geometric properties. Comput Methods Appl Mech Eng 193(1–2): 139–160
16. Papadopoulos V, Inglessis P (2007) The effect of non-uniformity of axial loading on the buckling behaviour of shells with random imperfections. Int J Solids Struct 44(18–19):6299–6317
17. Schenk CA, Schueller GI (2003) Buckling analysis of cylindrical shells with random geometric imperfections. Int J Non-Linear Mech 38:1119–1132
18. Schenk CA, Schueller GI (2005) Uncertainty assessment of large finite element systems. In: Pfeiffer F, Wriggers P (eds) Lecture notes in applied and Computational Mechanics. Springer, Heidelberg, p 24
19. Charmpis DC, Schuëller GI, Pellissetti MF (2007) The need for linking micromechanics of materials with stochastic finite elements: a challenge for materials science. Computat Mater Sci 41(1):27–37
20. Lagaros N, Papadopoulos V (2006) Optimum design of shell structures with random geometric, material and thickness imperfections. Int J Solids Struct 43(22–23):6948–6964
21. Schenk CA, Schueller GI, Arbocz J (2000) On the analysis of cylindrical shells with random imperfections. In: Papadrakakis M, Samartin A, Onate E (eds) Proceedings of fourth international colloquium on computation of shell and spatial structures. IASS-IACM 2000, Chania, Crete
22. Arbocz J, Abramovich H (1979) The initial imperfection data bank at the Delft University of Technology Part 1, Technical Report LR-290, Delft University of Technology, Department of Aerospace Engineering
23. Lin J, Zhao Y, Zhang Y (2001) Accurate and highly efficient algorithms for structural stationary/non-stationary random responses. Comput Methods Appl Mech Eng 191(1–2):103–111

24. Shinozuka M, Deodatis G (1996) Simulation of multi-dimensional Gaussian stochastic fields by spectral representation. Appl Mech Rev ASME 49:29–53
25. Argyris JH, Tenek L, Olofsson L (1997) TRIC, A simple but sophisticated 3node triangular element based on 6 rigid-body and 12 straining modes for fast computational simulations of arbitrary isotropic and laminated composite shells. Comput Methods Appl Mech Eng 145:11–85
26. Argyris JH, Tenek L, Papadrakakis M, Apostolopoulou D (1998) Postbuckling performance of the TRIC natural mode triangular element for isotropic and laminated composite shells. Comput Methods Appl Mech Eng 166:211–231
27. Argyris JH, Papadrakakis M, Stefanou G (2002) Stochastic Finite Element Analysis of Shells. Comput Methods Appl Mech Eng 191(41–42):4781–4804
28. Bathe K-J (1996) Finite element procedures. Prentice Hall, Englewood Cliffs
29. Szekely GS (1996) Random eigenvalue problems (literature review), internal working report, No.36–96, Institute of Engineering Mechanics, Leopold-Franzens Universitat, Innsbruck
30. Ghanem R, Ghosh D (2007) Efficient characterization of the random eigenvalue problem in a polynomial chaos decomposition. Int J Numer Methods Eng 72:486–504
31. Pradlwarter HJ, Schueller GI, Szekely GS (2002) Random eigenvalue problems for large systems. Comput Struct 80:2415–2424
32. Papadrakakis M, Yakoumidakis M (1987) A partial preconditioned conjugate gradient method for large eigenproblems. Comput Methods Appl Mech Eng 62:195–207
33. Papadrakakis M, Yakoumidakis M (1987) On the preconditioned conjugate gradient method for solving $(\mathbf{A}\text{-}\lambda\mathbf{B})\mathbf{X} = 0$. Int J Numer Methods Eng 24:1355–1366
34. Papadrakakis M, Papadopoulos V (1996) Robust and efficient methods for stochastic finite element analysis using Monte Carlo simulation. Comput Methods Appl Mech Eng 134:325–340
35. Charmpis DC, Papadrakakis M (2005) Improving the computational efficiency in finite element analysis of shells with uncertain properties. Comput Methods Appl Mech Eng 194:1447–1478